

Study of energy backflow in unidirectional monochromatic and space-time waves

Peeter Saari^{1,2} and Ioannis Besieris³

¹*Institute of Physics, University of Tartu, W. Ostwaldi 1, 50411, Tartu, Estonia*

²*Estonian Academy of Sciences, Kohtu 6, 10130 Tallinn, Estonia and*

³*The Bradley Department of Electrical and Computer Engineering,
Virginia Polytechnic Institute and State University, Blacksburg, Virginia 24060, USA**

(Dated: May 6, 2024)

Backflow, or retropropagation, is a counterintuitive phenomenon whereby for a forward-propagating wave the energy locally propagates backward. In this study, energy backflow has been examined in connection with (a) (2+1)-dimensional unidirectional scalar and vector-valued monochromatic waves; (b) a (2+1)D scalar spatiotemporal wavepacket constructed by using an appropriate temporal frequency spectrum; (c) a scalar closed-form analytical unidirectional version of the Focus Wave Mode—a localized pulse propagating luminally and without spread. Furthermore, an extended class of (2+1)D and (3+1)D finite-energy unidirectional spatiotemporally localized wave packets has been derived.

PACS numbers: 03.50.De, 41.20.Jb, 42.25.Bs, 42.25.Fx

I. I INTRODUCTION

The phenomenon of backflow takes place when some quantity (energy density flow, local momentum, probability flow, etc.) in some spatio-temporal region of a wavefield is directed backward with respect to the directions of all plane-wave constituents of the wavefield. Backflow is a wave phenomenon that may occur in all kinds of wavefields describable by different types of wave equations [1]. Position probability backflow specific to quantum particles, such as electrons, has been termed ‘quantum backflow,’ and this subject is actively studied (see a review [2] and references therein). Recently, the similarities and differences between quantum backflow and backflow in classical wavefields has been discussed intensively [1, 3–5].

It has been known for quite a long time that in a superposition of four appropriately polarized and directed electromagnetic plane waves the Poynting vector direction can be reversed with respect to the direction of propagation of the resultant wave and its constituents [6]. A rather prominent energy backflow exhibited in such a quartet of electromagnetic waves was investigated recently in detail [7, 8]. In the physical optics community the energy backflow in sharply focused light has been known more than half a century and has been thoroughly studied theoretically recently [9–11]. In the context of quantum backflow, monochromatic optical fields have been used for recent experimental verification of the effect [12, 13]. Energy backflow in electromagnetic Bessel beams has been analytically demonstrated in [14, 15]; also, in pulsed electromagnetic X waves [16]. Important is the circumstance that the backflow appears only in certain polarization geometries and occurs neither in scalar Bessel beams nor in a scalar X wave. The latter belongs

to the class of the so-called nondiffracting (nonspreading, propagation-invariant) localized waves (LWs)—also known as space-time wave packets (STWP), especially their 2-dimensional versions—which have been studied intensively during the past thirty years (see, e.g., [17–35]). They constitute spatiotemporally localized solutions to various hyperbolic equations governing acoustic, electromagnetic and quantum wave phenomena and can be classified according to their group velocity as luminal LWs, or focus wave modes (FWM), superluminal LWs, or X waves (XWs), and subluminal LWs. Overviews of theoretical and experimental studies can be found in two edited monographs on the subject [36, 37] and in the recent thorough review article [38].

From the point of view of the backflow phenomenon it is principally crucial whether the plane-wave constituents of the wavepacket propagate only in the positive, say z -direction or also backward. In other words, whether the support of the spectrum in the wavenumber space is restricted to the positive half-space only of the z -component of the wavevector. In this case the wave—we call it unidirectional—can be launched from an aperture as a freely propagating beam and the very question of energy backflow is meaningful. It must be pointed out that, in general, the group velocity in a wave packet typically differs from the energy velocity, see [39, 40].

In [41] a number of exact localized solutions to the wave equation which are totally free of backward components were found. In [42] a simple analytic expression for a unidirectional finite-energy pulse was determined. However, occurrence of possible backflow was not considered in these papers. Using as an example of a particular version of the expression of a hopfion-like unidirectional pulse, backflow was shown explicitly in [1]. In our work [43] we studied the backflow in scalar-valued and vector-valued generalizations of this propagation-variant (focusing) pulse. Additional generalizations of the unidirectional hopfion-like propagation-variant finite-energy pulses have been introduced by Lekner in [44].

* Corresponding author: peeter.saari@ut.ee

The aim of this paper, which is in a sense a follow-up to [43], is to study the phenomenon of energy backflow in a new (2+1)-dimensional unidirectional field, in a unidirectional version of a well-known propagation-*invariant* localized wave, and to find new expressions for an extended class of unidirectional waves.

The paper is organized as follows. In the next section we introduce a new solution to the Helmholtz equation in two dimensions—an exceptional successful result of our search for closed-form expressions of unidirectional monochromatic wavefields. The corresponding harmonically time-dependent wave field turns out to possess rather remarkable backflow. It is known that a spherically symmetric monochromatic 3-dimensional standing wave transforms to a propagation-invariant subluminal LW if observed from another inertial reference frame—to the so-called deBroglie-MacKinnon (dBM) pulse [45],[24],[27]. Lorentz transformations of our solution results in a (2+1)-dimensional version of the dBM pulse, the backflow in which we consider at the end of the section.

In Section III we consider the space-time wave packet formed from the monochromatic constituents introduced in the preceding section. Our interest in the (2+1)D field was motivated by three reasons: (i) it is an exceptional novel solution, (ii) launching of a 2-dimensional version of the dBM pulse and (iii) realization of Lorentz boosts of (2+1)D space-time wavepackets were experimentally demonstrated recently [46], (see also [47]), [48].

Section IV is devoted to the backflow in the so-called focus wave mode (FWM)—a luminal pulse (i.e., its group velocity is c in empty space) propagating without spreading, which is the most investigated LW in the literature. The FWM possesses a simple closed-form expression but has considerable contributions from backward propagating ('non-causal') plane wave constituents and is therefore non-interesting from the point of view of backflow study. Fortunately, although not simple but still a closed-form expression for a *unidirectional* version of FWM has been found [49] which has a remarkable backflow as will be shown in Section III.

In Section V we present new (2+1)D and (3+1)D closed-form expressions for an extended class of finite-energy unidirectional waves.

II. A (2+1)-DIMENSIONAL UNIDIRECTIONAL MONOCHROMATIC WAVE

In this section we consider 2-dimensional monochromatic waves of frequency $\omega = ck$, and therefore start with a general solution to the 2D Helmholtz equation independent of the y -coordinate

$$\begin{aligned} W(x, z) &= \int dk_x e^{-ik_x x} \\ &\times \int dk_z e^{-ik_z z} \delta(k_x^2 + k_z^2 - \frac{\omega^2}{c^2}) G(k_x, k_z) \\ &= \int_{-\omega/c}^{\omega/c} dk_z e^{-ik_z z} \frac{\cos Kx}{K} G(k_z). \end{aligned} \quad (1)$$

Here, k_x and k_z are corresponding components of the wave vector \mathbf{k} , and delta is the Dirac delta function which takes into account the dispersion relation. Resolving and integrating with respect to k_x results in the band-limited Fourier transform of the product $G(k_z)K^{-1} \cos Kx$, where $K = \sqrt{\omega^2/c^2 - k_z^2} \equiv \sqrt{k^2 - k_z^2}$ and $G(k_z)$ is a spectral amplitude function. If $G(k_z) = \text{const} = \pi^{-1}$ (for normalization), the Fourier transform is well-known and we get finally

$$W_0(x, z) = J_0\left(\frac{\omega}{c} \sqrt{x^2 + z^2}\right) = J_0(k\rho), \quad (2)$$

where J_0 is the the 0-th order Bessel function of the first kind, and in the last equality the radial coordinate $\rho = \sqrt{x^2 + z^2}$ of the cylindrical system has been introduced (see also [47]). Thus, the field has cylindrical symmetry with respect to the axis y . The symmetry results from the omnidirectional angular spectrum.

A. A new unidirectional wave

Our aim is to find an analytic (closed-form) expression of a unidirectional wave. This means that in Eq. (1) the condition $G(k_z) = 0$ must be fulfilled for $k_z < 0$ or $G(k_z) = \theta(k_z)\theta(k - k_z)G(k_z)$, where $\theta(\cdot)$ is the Heaviside unit step function. The only closed-form expression for the integral with a unidirectional spectrum we could find was a combination of cosine and sine transforms with respect to k_z in [50], Sect.1.7, Eq. (46) and Sect. 2.7, Eq. (32), *viz.*,

$$\begin{aligned} W(x, z) &= \mathcal{F}_{\cos} \left\{ \theta(k - k_z) \frac{\sqrt{k} \cos\left(x\sqrt{k^2 - k_z^2}\right)}{\sqrt{k_z} \sqrt{k^2 - k_z^2}} \right\} \\ &+ i\mathcal{F}_{\sin} \left\{ \theta(k - k_z) \frac{\sqrt{k} \cos\left(x\sqrt{k^2 - k_z^2}\right)}{\sqrt{k_z} \sqrt{k^2 - k_z^2}} \right\}, \end{aligned} \quad (3)$$

which yields the following expression with Bessel functions of fractional orders

$$W(x, z) = C\sqrt{k|z|} \left\{ \begin{array}{l} J_{-\frac{1}{4}}\left[\frac{k}{2}(\sqrt{x^2 + z^2} - x)\right] \\ \times J_{-\frac{1}{4}}\left[\frac{k}{2}(\sqrt{x^2 + z^2} + x)\right] \\ + i \text{signum}(z) \\ \times J_{\frac{1}{4}}\left[\frac{k}{2}(\sqrt{x^2 + z^2} - x)\right] \\ \times J_{\frac{1}{4}}\left[\frac{k}{2}(\sqrt{x^2 + z^2} + x)\right] \end{array} \right\}. \quad (4)$$

Here, in order to ensure normalization of the field to unity at the origin, we have introduced the constant $C = \Gamma(3/4)^2/2 \approx 0.75$, where Γ is the gamma-function. The factor \sqrt{k} has been introduced into the spectrum in Eq. (3) for making $W(x, z)$ dimensionless. It is important to notice that as the arguments of the Bessel functions are non-negative, they have no imaginary parts and a simple complex conjugation symmetry holds $W(x, z < 0) = W^*(x, z > 0)$ in accordance with Eq. (1) if there the lower integration limit is set to zero and $G(k_z)$ is a real-valued function.

Since $J_{-\frac{1}{4}}(z)$ diverges at $z = 0$, Eq. (4) is not suitable for expressing the field along the axis x . Instead, we evaluated the corresponding integral

$$W(x, 0) = \sqrt{k} \int_0^k dk_z \frac{\cos Kx}{\sqrt{k_z K}} = \int_0^{\pi/2} d\phi \frac{\cos(kx \sin \phi)}{\sqrt{\cos \phi}}. \quad (5)$$

The second integral results from the variable transformation $k_z = k \cos \phi$. We see that the angular spectrum, or the density of directions of the plane-wave constituents, varies as $1/\sqrt{\cos \phi}$ and is infinitely strong for the plane waves falling perpendicularly to the axis z while the integral of the spectrum is finite. This is analogous to the case of the field of two superposed plane waves falling under the angle ϕ_0 onto the axis z when the spectrum is $\delta(\phi - \phi_0)$, i.e., diverging, but the field turns out to be finite. The other diverging factor in Eq. (1), $K^{-1} = (k^2 - k_z^2)^{-1/2} = (k \sin \phi)^{-1/2}$ takes into account the infinite growth of density of plane wave directions per dk_z if $k_z \rightarrow k$, but it cancels out in the change of the integration variable to ϕ .

The last integral in Eq. (5) has the following analytic solution

$$W(x, 0) = C \left(\frac{kx}{2} \right)^{\frac{1}{4}} \frac{3J_{\frac{3}{4}}(kx) - 2kx J_{\frac{7}{4}}(kx)}{\Gamma(\frac{3}{4}) kx}. \quad (6)$$

We evaluated and checked the correctness of Eqs. (4) and (6) with the help of three different software packages for scientific computations, also by direct numerical integration of Eq. (3), as well as by subjecting the field to the Helmholtz equation.

The modulus squared of the wavefunction given by Eqs. (4), (6) is plotted in Fig. 1. As it is obvious from Eq. (4), the real part of $W(x, z)$ is even and the imaginary part is odd with respect to the variable z , and both are even with respect to x . Therefore $W(x, 0)$ must be also even with respect to x and purely real irrespective of the sign of x . The latter features are not directly seen from Eq. (6) but an analysis proves their trueness.

To our best knowledge, the unidirectional 2D monochromatic wavefunction given in Eq. (4) is studied here for the first time.

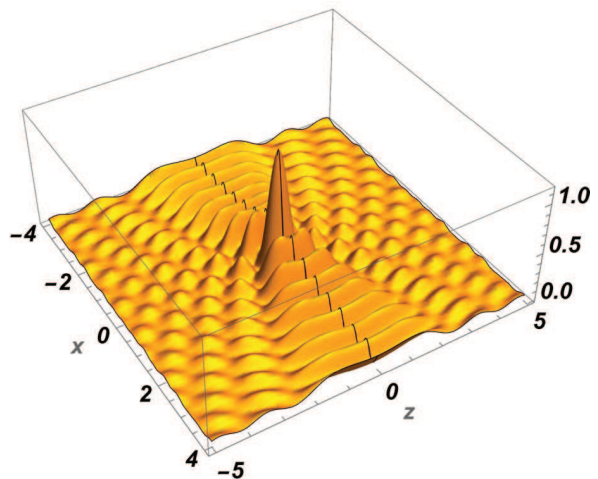


FIG. 1. Plot of the modulus squared $|W(x, z)|^2$ with $k = 2\pi$. The black line corresponds to $|W(x, 0)|^2$.

B. Backflow in the unidirectional scalar wave

To get a full space-time wavefunction, the time exponential factor $\exp(-ikct)$ must be added to the spatial functions. In the case of Eq. (2) this results in a cylindrical standing wave. However, Eq. (4) is a complex-valued function, i.e., contains a non-zero phase which with the time exponent results in a propagating phase. We found the phase velocity along the axis z by evaluating $\Phi(z) = \arctan[\text{Im } W(0, z)/\text{Re } W(0, z)]$. The phase $\Phi(z)$ turned out to be in good approximation linear with respect to z : the first term in the series expansion at $z = 0$ is $2\pi^{-2}\Gamma(3/4)^4 kz \approx 0.457 kz$ while the next term is $-0.0013 (kz)^3$, i.e., much smaller at least if $kz \leq 2\pi$. Hence, the phase velocity $v_{ph} \approx 2.2c$ and this value does not depend on the value of the wave vector k . This can be understood if one notices that in the case of angular spectrum $(\cos \phi)^{-1/2}$ the average angle is about 1 rad and a plane wave falling onto the z -axis under such angle has the superluminal phase velocity just about $2c$ along the z -axis.

Our unidirectional wave undergoes propagation and it makes sense to calculate the energy flow using the following definitions for the Poynting vector and the energy density of a complex scalar field:

$$\mathbf{P} = -\frac{1}{2}(\partial_{ct}\Psi^*)(\nabla\Psi) - \frac{1}{2}(\partial_{ct}\Psi)(\nabla\Psi^*), \quad (7)$$

$$u = \frac{1}{2}(\partial_{ct}\Psi)(\partial_{ct}^*\Psi) + \frac{1}{2}(\nabla\Psi) \cdot (\nabla\Psi^*). \quad (8)$$

The energy velocity is defined as $\mathbf{V} = \mathbf{P}/u$. For the field $\Psi(x, z, t) = W(x, z) \exp(-ikct)$ the z -component of the Poynting vector is shown in Fig. 2.

The dimensionless wave vector $k = \pi$, and, correspondingly, the length unit is half of the wavelength $\lambda = 2\pi/k = 2$. The time instant $ct = 0.5$. However, in

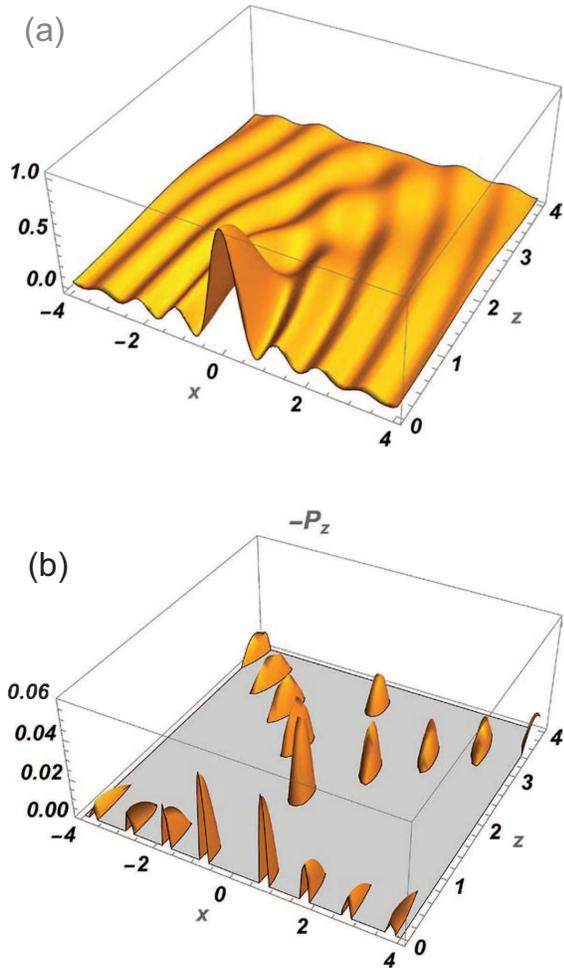


FIG. 2. a, spatial dependence of the z -component of the Poynting vector of the complex-valued field $\Psi(x, z, t) = W(x, z) \exp(-ikct)$ according to Eq. (7). b, the same for its negative values (backflow). $k = \pi$. Vertical axes have been normalized to unity at maximum of P_z

. Notice, that, unlike Fig. 1, the plots cover only the positive z -axis.

distinction from the case of the real versions of the field $\text{Re}\{\Psi(x, z, t)\}$ and $\text{Im}\{\Psi(x, z, t)\}$, neither the Poynting vector nor the energy density of the complex-valued field $\Psi(x, z, t)$ depend on time as is true of monochromatic wave fields in general. The dimensionless coordinates allow to adopt easily the plots for optical, microwave or acoustic frequency ranges. For example, if we took the length unit equal to $0.25 \mu\text{m}$, the wavelength would be $0.5 \mu\text{m}$, which is in the middle of the optical region, and the time instant $ct = 0.5$ would correspond to $t \approx 0.4$ femtosec.

The plots in Fig. 2 and 3 demonstrate remarkable backflow—up to 5% from the maximal forward flow. As Fig. 3a shows, in the backflow maximum region with coordinates $(0, 1.6)$ the backflow velocity reaches about

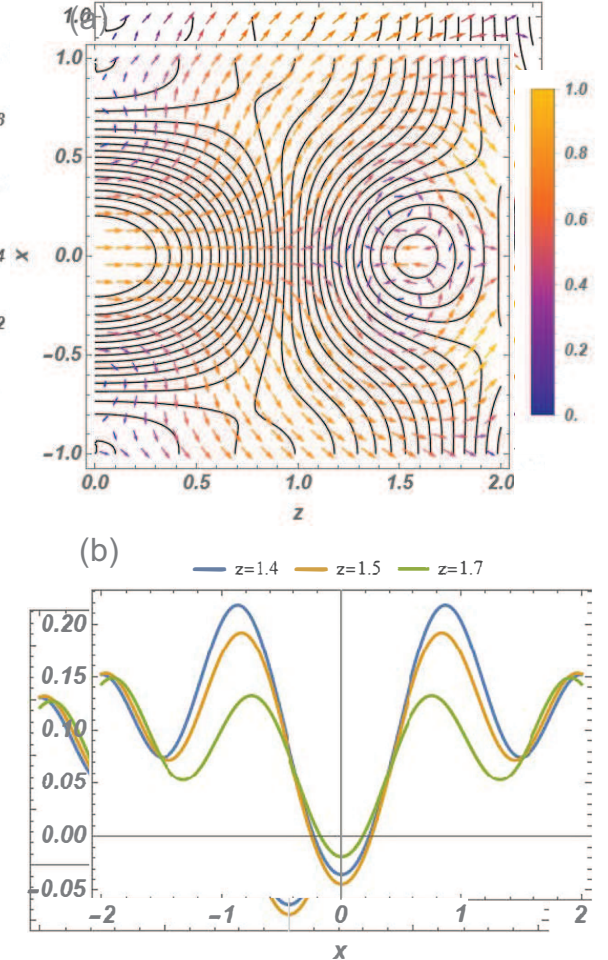


FIG. 3. a, contour plot of the energy density according to Eq. (8) superimposed by the vector field plot of the energy velocity \mathbf{V} , the color bar showing values of the velocity in the range $0 \dots c$, where $c = 1$ is the speed of light (or sound in the case of acoustical wave). b, 2D intersections of the plot Fig. 2a of the z -component of the Poynting vector.

80% of c . We do not present the plots here, but the same holds for wavefields $\text{Re}\{\Psi(x, z, t)\}$ and $\text{Im}\{\Psi(x, z, t)\}$, the backflow being even somewhat stronger in the latter. The Poynting vector and energy density of a complex-valued field are vectorial sums of those of its real and imaginary constituents fields, but if the regions of backflow in the two constituents do not overlap, mutual cancellation takes place and weaker backflow may disappear.

C. Backflow in the unidirectional vector-valued wave

We used the same procedure of computing the Poynting vector and energy density of the electromagnetic field corresponding to a scalar field as in our previous paper [43]. Shortly, the scalar field $\Psi(x, z, t) =$

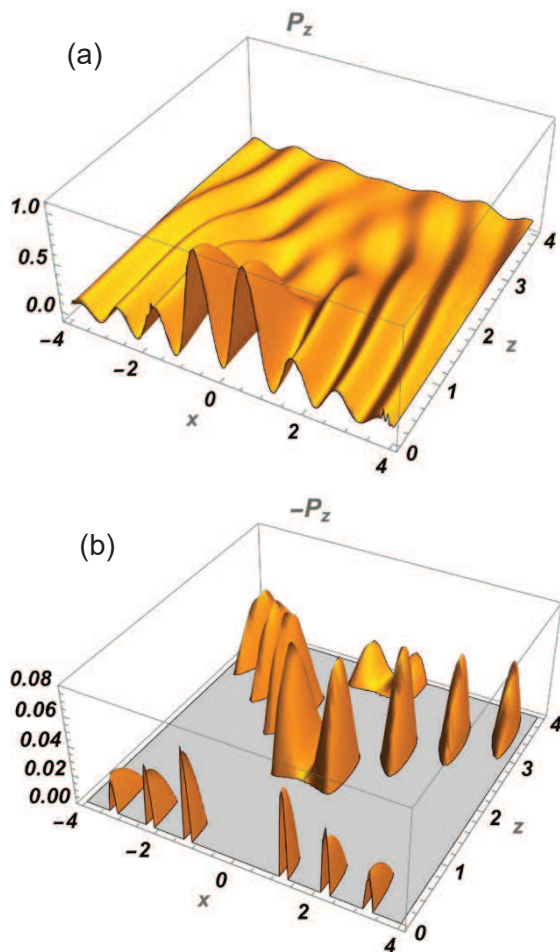


FIG. 4. a, spatial dependence of the z -component of the Poynting vector of the electromagnetic field. b, the same for its negative values (backflow). See also caption of Fig. 2.

$W(x, z) \exp(-ikct)$ was ascribed to the z -component of the Hertz vector $\vec{\Pi} = \Psi(x, z, t) \vec{e}_z$, from which the Riemann-Silberstein vector

$$\vec{F} = \nabla \times \nabla \times \vec{\Pi} + (i/c) \nabla \times \left(\partial \vec{\Pi} / \partial t \right) \quad (9)$$

was obtained. In turn, the latter is related to the Poynting vector as $\vec{P} = \vec{E} \times \vec{H} = -i\vec{F} \times \vec{F}^*$. The results are presented in Figs. 4 and 5.

A stronger backflow can be noticed. This is in agreement with earlier observation that polarization may enhance the backflow [7, 8, 16]. We draw attention to the vortices of the velocity vector field in the right corners of Fig. 5a.

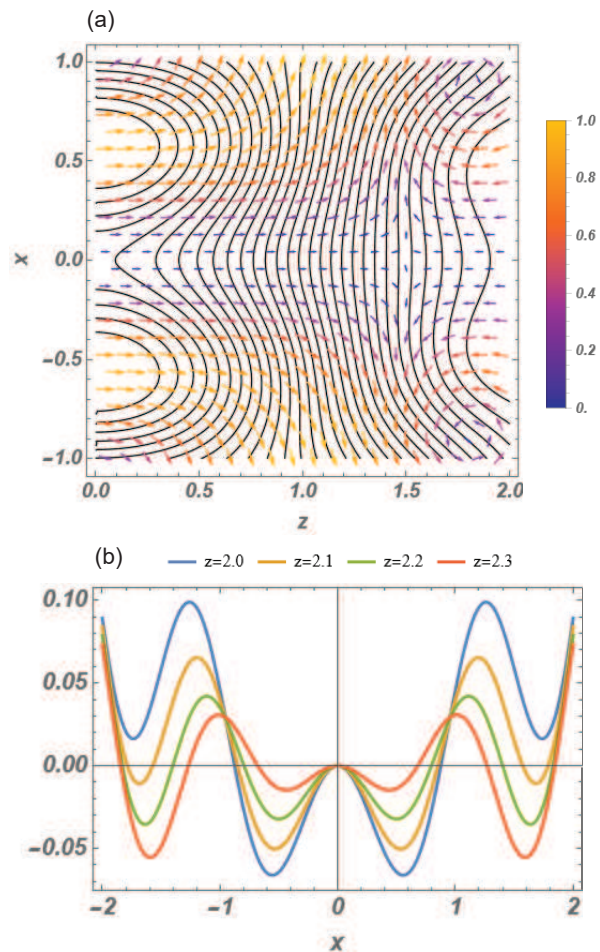


FIG. 5. a, contour plot of the energy density $\vec{F} \cdot \vec{F}^*$ superimposed on the vector field plot of energy velocity. b, plots of the z -component of the Poynting vector. b, 2D intersections of the plot Fig. 4a of the z -component of the Poynting vector.

D. Relativistic boosting—2D deBroglie-MacKinnon pulse

Another way to get a time-dependent wave from a localized solution of the Helmholtz equation is the Lorentz transformation of the variables z and t of a monochromatic wave, which results in a sub-luminally propagating pulse. In the case of the 3D spherically symmetric standing wave given by $\sin(k\sqrt{x^2 + y^2 + z^2}) / k\sqrt{x^2 + y^2 + z^2} \exp(-ikct)$, this procedure leads to the de Broglie-MacKinnon (dBm) pulse [24],[27], and in the case of the cylindrically symmetric wavefunction in Eq. (2)—to a 2D version of the dBm pulse. Lorentz transforming of z and t in $W(x, z) \exp(-ikct)$ leads also to a subluminal pulse. However, the backflow effect in such field is weaker the closer is the pulse group velocity to the speed of light, and we do not present the plots here. The reason is due to the relativistic aberration effect; the propagation directions

of the plane wave constituents are compressed towards the axis z and away from the perpendicular to it (see Fig. 10 in [27]), while the contribution of a plane wave constituent in the backflow has the tendency to grow with the angle of inclination of its direction with respect to the axis z [8]. On the other hand, one might suppose that due to the aberration effect the ring-shaped support of the spectrum of a dBM pulse becomes stretched along the k_z -axis into an ellipse which no longer extends to the negative values of k_z . However, under the Lorentz transformation the most negative value of $k_z = -k$ becomes $k'_z = (1 - v^2/c^2)^{-1/2}(v/c - 1)k$, i.e., it cannot become positive at any realistic boosting speed v .

III. A (2+1)-DIMENSIONAL UNIDIRECTIONAL SPACE-TIME WAVE PACKET

A closed-form analytical solution seems relatively difficult to obtain by using an appropriate superposition of the (2+1)D solution in Eq. (4) over the wavenumber k . The same can be said of Lekner's (3+1)D monochromatic unidirectional solution [51]. However, this does not mean that (2+1)D or (3+1)D spatiotemporally localized unidirectional closed-form solutions do not exist.

Indeed, the monochromatic (2+1)D field $\Psi(x, z, t) = W(x, z) \exp(-ikct)$ can be integrated over k using the spectrum $\exp(-ak)\sqrt{a/k}$, where $a > 0$ is the pulsewidth parameter, with the help of the table integral 6.612-3 in [52] (see also note to Ref.[52]). The result turns out to be a closed-form expression with the Legendre functions of the second kind $Q_\nu(\cdot)$, and for $z > 0$ it reads

$$\begin{aligned} \Phi(x, z, t) = & \\ & = \sqrt{\frac{\pi a}{2z}} Q_{-\frac{3}{4}} \left(2z^{-2} \left[x^2 + \frac{1}{2}z^2 + (a + ict)^2 \right] \right) \\ & + i\sqrt{\frac{\pi a}{2z}} Q_{-\frac{1}{4}} \left(2z^{-2} \left[x^2 + \frac{1}{2}z^2 + (a + ict)^2 \right] \right). \end{aligned} \quad (10)$$

The special functions $Q_\nu(\cdot)$ with complicated arguments make the solution rather cumbersome but still it is analytical and allows taking derivatives needed for calculation of the Poynting vector, as well as electromagnetic fields. To our best knowledge, the expression in Eq. (10) of a (2+1)D unidirectional time-space wave packet is published here for the first time.

At the instant $t = 0$ the pulse is narrow in the x -direction, see Fig. 6a. With time it acquires a crater-like shape, radius of the circular edge of which increases with the speed of light (Fig. 6b). Since the angular spectrum is the strongest in directions perpendicular to the axis z , the "crater" develops on the "ridge" along the z -axis.

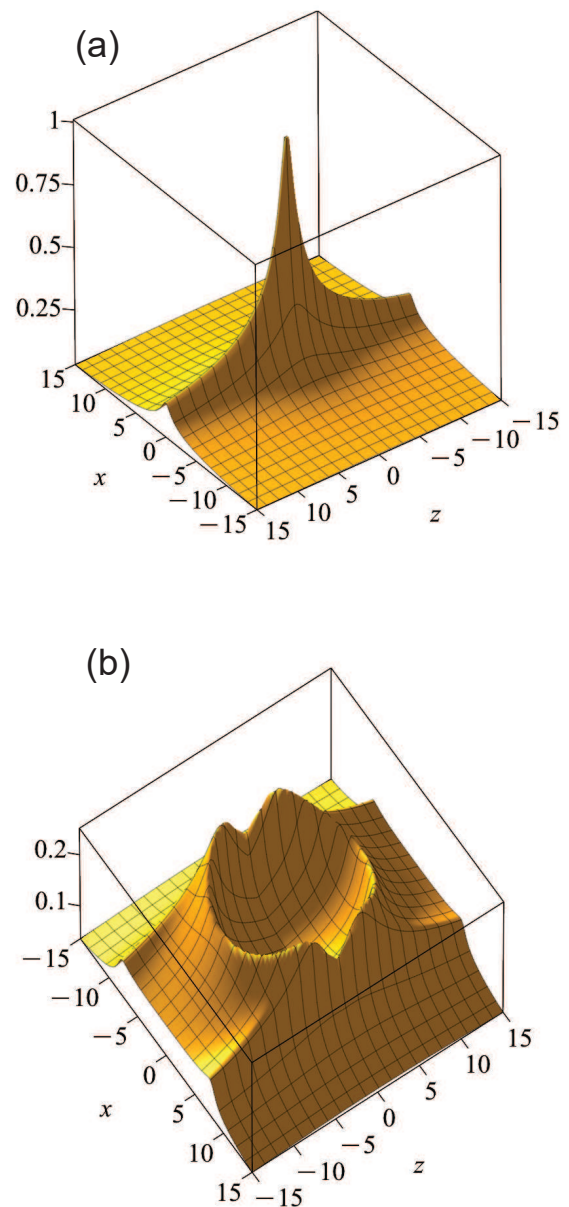


FIG. 6. Square modulus of the wave packet in Eq. (10) at (a) $t = 0$ and (b) $t = 8$. $a = 1/2$, $c = 1$.

The z -component of its Poynting vector evaluated according to the real-valued version of Eq. (7) is depicted in Fig. 7. The forward energy flow is the strongest along the edge of the "crater". The backflow is of the same order of magnitude as in the case of the monochromatic field.

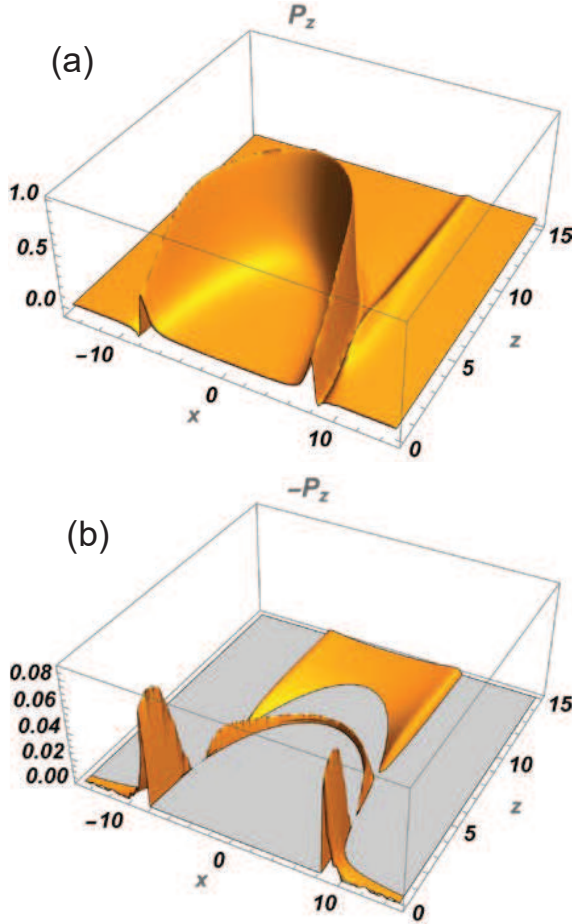


FIG. 7. a, spatial dependence of the z -component of the Poynting vector of the real part of field $\Phi(x, z, t)$. b, the same for its negative values (backflow). Notice, that the plots cover only the positive z -axis. $t = 8$. $a = 1/2$, $c = 1$

IV. A (3+1)D UNIDIRECTIONAL VERSION OF THE LUMINAL FOCUS WAVE MODE

The rather complicated closed-form expression for a *unidirectional* version of FWM, which contains Lommel functions of two arguments, has been derived in [49]. The field of the pulse can be written in cylindrical coordinates as the following difference:

$$U_{k_1, \infty}(\rho, z, t) = U_{k_0, \infty}(\rho, z, t) - U_{k_0, k_1}(\rho, z, t). \quad (11)$$

Here $U_{k_0, \infty}(\rho, z, t)$ is the known expression of the FWM which is obtained by superposing all Bessel-beam constituents with wavenumbers k from the minimal value k_0 up to infinity. This means that in the superposition the corresponding integration for the z -component of the wavenumber runs over the range $k_z \in (-k_0, \infty)$, i.e., the FWM contains considerable contribution from the backward-propagating constituents. Eq. (11) states that if we subtract from the FWM a field obtained as a super-

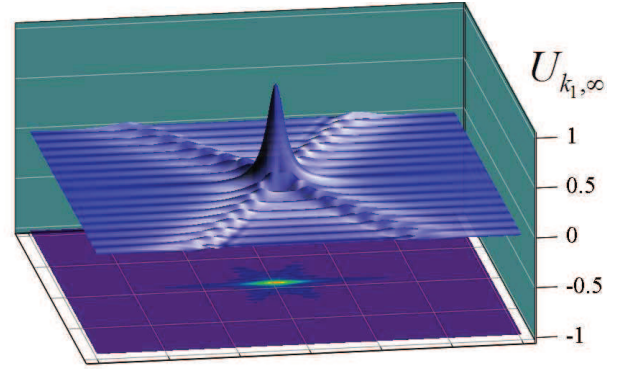


FIG. 8. The real part (upper surface plot) and the modulus (pseudocoloured contour plot on the basal plane) of the wavefunction of the unidirectional FWM $U_{k_1, \infty}(\rho, z, t)$ in dependence on the coordinate z (increasing from the left to the right) and on a transverse coordinate $x = \pm\rho$. The distance between the grid lines on the basal plane (x, z) is $4\lambda_1$, $\lambda_1 = 2\pi/k_1$. Pulswidth parameter $z_0 = 2\lambda_1/\pi$, time instant $t = 0$. Reproduced from [49].

position of the constituents with k from k_0 up to a value k_1 which corresponds to nonnegative k_z , then we get the expression of the unidirectional field $U_{k_1, \infty}(\rho, z, t)$ we are looking for. The subtracted field $U_{k_0, k_1}(\rho, z, t)$ is the one which is expressed in terms of the Lommel functions. Choosing $k_1 = 2k_0$, the integration for the z -component runs over the range $k_z \in (0, \infty)$, i.e., the difference field $U_{k_1, \infty}(\rho, z, t)$ contains all forward-propagating Bessel-beam constituents [49].

The field $U_{k_1, \infty}(\rho, z, t)$ is depicted in Fig. 8. In $U_{k_0, \infty}(\rho, z, t)$ the backward propagating Bessel-beam constituents have the strongest weight and, correspondingly, the phase of the field propagates backward along the axis z , i.e., in opposite direction with respect to the pulse's (group) velocity (see animations in Suppl. Mat. of Ref. [49]). In $U_{k_1, \infty}(\rho, z, t)$ the strongest weight belongs to the plane wave constituents propagating nearly perpendicularly with respect to the axis z and, correspondingly, the equiphasal surfaces are cylinders coaxial with respect to the axis z , which have radial period about $\lambda_1 = 2\pi/k_1$ as seen in Fig. 8.

Fig. 9 depicts the z -component of the Poynting vector of the real scalar-valued field $\Phi = \text{Im}\{U_{k_1, \infty}(\rho, z, t)\}$, which has been calculated with the help of the real-valued version of Eq. (7) $\mathbf{P} = -(\partial_{ct}\Phi)(\nabla\Phi)$. As seen in Fig. 9, there are two strongest backflow maxima—about 3% of the peak values of forward flow—in the propagation axis z . Backflow peaks in the field $\text{Re}\{U_{k_1, \infty}(\rho, z, t)\}$ are by an order of magnitude weaker at $t = 0$ but become pretty much similar to those in Fig. 9 for a shifted time instant $ct = \pm 0.25$ which corresponds to $\pm 1/4$ of the period $T = 2\pi/ck_1$. This is understandable, since such a quarter-cycle temporal shift not only moves the pulse along the z -axis with velocity c but also transforms the field $\text{Re}\{U_{k_1, \infty}(\rho, z, t)\}$ approximately into $\text{Im}\{U_{k_1, \infty}(\rho, z, t)\}$ and *vice versa*.

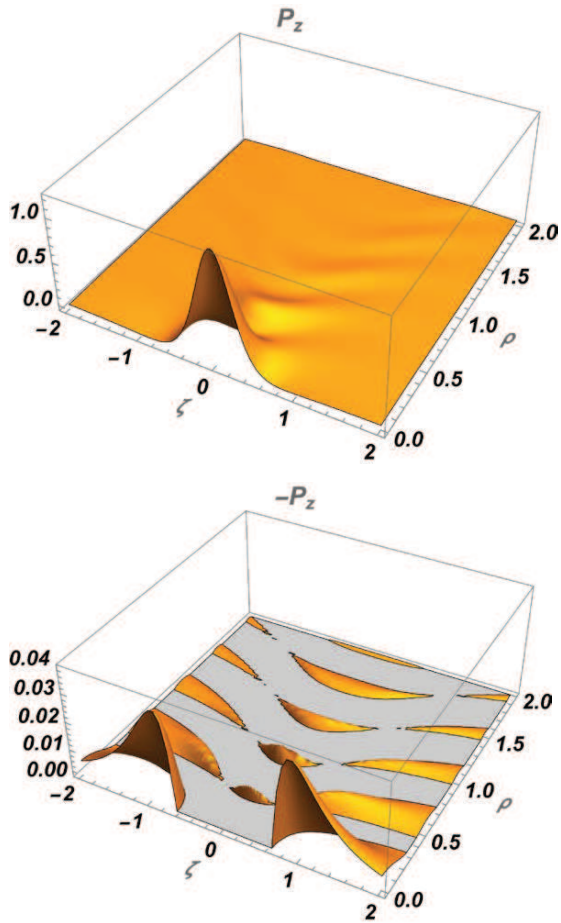


FIG. 9. a, spatial dependence of the z -component of the Poynting vector of $\text{Im}\{U_{k_1, \infty}(\rho, z, t)\}$. b, the same for its negative values (backflow). $\zeta \equiv z - ct$, $k_0 = \pi$, $k_1 = 2\pi$, $c = 1$, $t = 0$. Notice that the orientation of the 3D plots differs from that of preceding figures.

V. AN EXTENDED CLASS OF FINITE-ENERGY (2+1)D AND (3+1)D UNIDIRECTIONAL SPATIOTEMPORALLY LOCALIZED WAVES

It was pointed out in Section II that the unidirectional ('causal') monochromatic (2+1)D solution $\Psi(x, z, t) = W(x, z) \exp(-ikct)$ is unique. An interesting question is whether the same applies to (3+1)D monochromatic solutions and to space-time packets. To answer this question, we start with the following Fourier synthesis of a general solution of the homogeneous scalar wave equation in (3+1)D free space.

$$\begin{aligned} \psi(\rho, \phi, z, t) = & \exp(im\phi) \int_0^\infty dk \exp(-ikct) \int_0^k dk_z \\ & \times \exp(ik_z z) J_m(\rho \sqrt{k^2 - k_z^2}) F(k, k_z). \end{aligned} \quad (12)$$

For $m = 0$ and using the spectrum $F(k, k_z) = \delta(k - k_0) k_z \exp(bk_z)$ Lekner [51] has derived a (3+1)D monochromatic unidirectional wave expressed in terms of Lommel functions. Energy backflow is present, but it is very weak.

Under the constraint $k_z = k \cos \theta$ in Eq. (12), we obtain

$$\begin{aligned} \psi(\rho, \phi, z, t) = & \exp(im\phi) \int_0^\infty dk J_m(\rho k \sin \theta) \\ & \times \exp\{-ik \cos \theta [z - (c/\cos \theta) t]\} F_1(k). \end{aligned} \quad (13)$$

This is a superposition of causal monochromatic Bessel beams propagating along the z -direction with the superluminal speed $v = c/\cos \theta$. These Bessel beams exhibit energy backflow only at a vector-valued level [15]. Using the spectrum $F(k) = \exp(-ka \cos \theta) k^m$ in Eq. (13) gives rise to the infinite-energy unidirectional m -order azimuthally asymmetric X wave

$$\begin{aligned} \psi(\rho, \phi, z, t) = & (2^m/\sqrt{\pi}) \Gamma(m + 1/2) \\ & \times \frac{\exp(im\phi) \rho^m}{(\rho^2 \sin^2 \theta + \cos^2 \theta (a + i(z - ct/\cos \theta))^2)^{m + 1/2}}. \end{aligned} \quad (14)$$

which exhibits energy backflow only at a vector-valued level.

Let us demonstrate that integration over the wavenumber k (or temporal frequency) first adds a large class of closed-form expressions for unidirectional (2+1)D and (3+1)D finite-energy space-time wave packets.

Consider, specifically, the (2+1)D Fourier superposition

$$\begin{aligned} \psi(x, z, t) = & \int_0^\infty dk \exp(-ikct) \int_0^k dk_z \exp(ik_z z) \\ & \times \exp[-ix\sqrt{k^2 - k_z^2}] F(k, k_z). \end{aligned} \quad (15)$$

Instead of performing the integration over k_z as it was done in Section II, let us interchange the order of integration and use the spectrum

$$\begin{aligned} F(k, z) = & 0, \quad 0 < k < k_z, \\ F(k, z) = & \sqrt{2/\pi} \frac{\exp(-a_1 k)}{(k + k_z)^{1/2}} G(k_z), \quad k > k_z, \\ G(k_z) = & 0, \quad 0 < k_z < b, \\ = & \exp(-a_2 k_z) (k_z - b)^q, \quad k_z > b. \end{aligned}$$

From [50] Eqs. 5.6-28, 29 and 4.3-5, we obtain the finite-energy unidirectional solution

VI. CONCLUSIONS

$$\begin{aligned} \psi(x, z, t) &= \exp[-b \alpha(x, z, t)] \\ &\times \frac{1}{g(x, t)} \left(\frac{\alpha(x, z, t)^{1/2}}{\beta(x, z, t)^{q+1}} + ix \frac{\alpha(x, z, t)^{-1/2}}{\beta(x, z, t)^{q+1}} \right); \\ g(x, t) &= \sqrt{x^2 + (a_1 + ict)}, \\ \alpha(x, z, t) &= a_2 - iz + g(x, t), \\ \beta(x, z, t) &= a_1 + ict + g(x, t). \end{aligned}$$

To derive an analogous (3+1)D solution, we use in Eq. (12) the spectrum

$$\begin{aligned} F(k, k_z) &= \exp \left[-k_z \left(\frac{a_1 - a_2}{2} \right) \right] \exp \left[-k \left(\frac{a_1 + a_2}{2} \right) \right] \\ &\times (k - k_z)^{m/2} G(k_z); \\ G(k_z) &= 0, \quad 0 < k_z < b, \\ &= (k_z - b)^q, \quad k_z > b, \end{aligned}$$

where $a_{1,2}$ with $a_1 > a_2$ are positive free parameters. Then, the integration can be carried out explicitly yielding

$$\begin{aligned} \psi(\rho, \phi, z, t) &= \frac{1}{g(\rho, t)} \frac{\beta^m(\rho, \phi, z, t)}{\alpha^{q+1}(\rho, z, t)} \exp[-b \alpha(\rho, z, t)]; \\ g(\rho, t) &= \sqrt{\left(\frac{a_1 + a_2}{2} + ict \right)^2 + \rho^2}, \\ \alpha(\rho, z, t) &= \frac{a_1 - a_2}{2} - iz + g(\rho, t), \\ \beta(\rho, \phi, z, t) &= \frac{\exp(i\phi) \rho}{\left(\frac{a_1 + a_2}{2} + ict + g(\rho, t) \right)}. \end{aligned}$$

This is an extended family of (3+1)D finite-energy unidirectional spatiotemporally localized waves (see, also, Eq. (21) in Ref. [43], where energy backflow has been studied for special cases).

Wavefunctions formed of plane wave constituents propagating only in the positive, say z-direction are called unidirectional. If they contain finite energy, they can be launched causally from an aperture. Even if they have theoretically infinite energy, in reality a finite-size aperture results in their finite-energy approximations which differ from the theoretical wavefunctions only by off-axis edge effects. It is for unidirectional wavefunctions that the very question of energy backflow is meaningful.

In our previous work [43], we examined in detail the energy backflow of (3+1)D finite-energy spatiotemporally localized unidirectional wave packets. In this study, we started an investigation of (2+1)D monochromatic causal unidirectional waves. To our surprise, we found only one such analytical scalar wavefunction. It is expressed in terms of fractional Bessel functions of the first kind. We first examined the energy backflow of this monochromatic wavefunction, both at a scalar and vector-valued level. By means of a superposition using an appropriate temporal frequency spectrum, we determined a novel (2+1)D space-time wave packet and studied its energy backflow. The energy backflow level of the latter was the same as in the monochromatic case. We continued our study of energy backflow in the case of a unidirectional version of the luminal Focus Wave Mode, which is expressed in terms of Lommel functions. Finally, we derived an extended class of (2+1)D and (3+1)D finite-energy unidirectional spatiotemporally localized wave packets. The latter provides detailed proof for the expressions in Eq. (21) of our previous work [43].

The study of energy backflow of the vector-valued version of the unidirectional monochromatic wave $\Psi(x, z, t) = W(x, z) \exp(-ikct)$ in Section IIC was based on the Riemann-Silberstein complex vector that results in electric and magnetic fields that both have nonzero components (non-TE and non-TM). Although specific results have not been incorporated in this article, an examination of the Poynting vectors associated individually with pure TE and TM fields associated to the scalar wave $\Psi(x, z, t)$ shows the presence of energy backflow. This is altogether different from the cases of the superposition of four plane waves [5–8], Bessel beams [13, 14], and a pulsed electromagnetic X wave [15], all of which require a superposition of TE and TM fields for the appearance of energy backflow.

-
- [1] I. Białynicki-Birula, Z. Białynicki-Birula and S. Augustynowicz, Backflow in relativistic wave equations, *J. Phys. Math. Gen.* **55**, 255702 (2022).
- [2] A. J. Bracken, Probability flow for a free particle: new quantum effects, *Phys. Scr.* **96**, 045201 (2021).
- [3] M. Barbier, C. J. Fewster, A. Goussev, G. Morozov, S. C. L. Srivastava, Comment on "Backflow in relativistic wave equations", *J. Phys. A: Math. Theor.* **56**, 138003 (2023).
- [4] A. J. Bracken and G. F. Melloy, Comment on 'Backflow in relativistic wave equations' *J. Phys. A: Math. Theor.* **56**, 138002 (2023).
- [5] I. Białynicki-Birula, Z. Białynicka-Birula, and S. Augustynowicz, Reply to comments on 'Backflow in relativistic wave equations,' *J. Phys. A: Math. Theor.* **56**, 138001 (2023).

- [6] B. Z. Katsenelenbaum, What is the direction of the Poynting vector? *J. Commun., Technol. Electron.*, **42**, 119 (1997).
- [7] X.-L. You, C.-F. Li, Dependence of Poynting vector on state of polarization, arXiv:2009.04119 [physics.optics] 5 Jan 2021.
- [8] P. Saari and I. Besieris, Backward energy flow in simple four-wave electromagnetic fields, *Eur. J. Phys.* **42**, 055301 (2021).
- [9] B. Richards and E. Wolf, Electromagnetic diffraction in optical systems, II. Structure of the image field in an aplanatic system, *Proc. R. Soc. A* **253** 358 (1959).
- [10] V. V. Kotlyar, S. S. Stafeev, A. G. Nalimov, A. A. Kovalev, and A. P. Porfirev, Mechanism of formation of an inverse energy flow in a sharp focus, *Phys. Rev. A*, **101**, 033811 (2020).
- [11] H. Li, C. Wang, M. Tang, and A. Xinzhong, Controlled negative energy flow in the focus of a radial polarized optical beam, *Opt. Express* **28** 18607 (2020).
- [12] Y. Eliezer, T. Zacharias, and A. Bahabad, Observation of optical backflow, *Optica* **7**, 72 (2020).
- [13] A. Daniel, B. Ghosh, B. Gorzkowski, and R. Lapkiewicz, Azimuthal backflow in light carrying orbital angular momentum, *Optica* **10**, 1217-1222 (2023).
- [14] J. Turunen, A. T. Friberg, Self-imaging and propagation-invariance in electromagnetic fields, *Pure Appl. Opt.* **2**, 51 (1993).
- [15] A. V. Novitsky, D. V. Novitsky, Negative propagation of vector Bessel beams, *J. Opt. Soc. Am. A*, **24** 2844 (2007).
- [16] M. A. Salem and H. Bağcı, Energy flow characteristics of vector X-Waves, *Opt. Express* **19**, 8526 (2011).
- [17] J. N. Brittingham, Focus wave modes in homogeneous Maxwell equations: Transverse electric mode, *J. Appl. Phys.* **54**, 1179-1189 (1983).
- [18] A. P. Kiselev Modulated Gaussian beams, *Radio Phys. Quant. Electron.* **26**, 1014-1020 (1983).
- [19] R. W. Ziolkowski, Localized transmission of electromagnetic energy, *Phys. Rev. A* **39**, 2005-2033 (1989).
- [20] I. M. Besieris, A. M. Shaarawi and R. W. Ziolkowski, A bidirectional traveling plane wave representation of exact solutions of the scalar wave equation, *J. Math. Phys.* **30**, 1254-1269 (1989).
- [21] J. Y. Lu and J. F. Greenleaf, Nondiffracting X waves-exact solutions to the free space scalar wave equation and their finite aperture realization, *IEEE Trans. Ultrason. Ferroelectr. Freq. Contr.* **39**, 19-31 (1992).
- [22] R. W. Ziolkowski, I. M. Besieris and A. M. Shaarawi, Aperture realizations of the exact solutions to homogeneous-wave equations, *J. Opt. Soc. Am. A* **10**, 75-87 (1993).
- [23] P. Saari and K. Reivelt, Evidence of X-haped propagation-invariant localized light waves, *Phys. Rev. Lett.* **79**, 4135-4137 (1997).
- [24] I. M. Besieris, M. Abdel-Rahman, A. M. Shaaraw and A. Chatzipetros, Two fundamental representations of localized pulse solutions to the scalar wave equation, *Progr. Electromagn. Res. (PIER)* **19**, 1-48 (1998).
- [25] J. Salo, J. Fagerholm, A. T. Friberg and M. M. Saloma, Unified description of X and Y waves, *Phys. Rev. E* **62**, 4261 (2000).
- [26] R. Grunwald, V. Kebbel, U. Neumann, A. Kummrow, M. Rini, R. T. Nibbering, M. Piche, G. Rousseau and M. Fortin, Generation and characterization of spatially and temporally localized few-cycle optical wave packets, *Phys. Rev. A* **67**, 063820-1-5 (2003).
- [27] P. Saari and K. Reivelt, Generation and classification of localized waves by Lorentz transformations in Fourier space, *Phys. Rev. E* **69**, 036612-1-12 (2004).
- [28] S. Longhi, Spatial-temporal Gauss-Laguerre waves in dispersive media, *Phys. Rev. E* **68**, 066612 1-6 (2003).
- [29] C. Conti, S. Trillo, P. di Trapani, G. Valiulis, A. Piskarskas, O. Jedrkiewicz, and J. Trull, Nonlinear electromagnetic X waves, *Phys. Rev. Lett.* **90**, 170406 1-4 (2003).
- [30] A. P. Kiselev, Localized light waves: Paraxial and exact solutions of the wave equation (review), *Opt. Spectrosc.* **102**, 603-622 (2007).
- [31] M. Yessemov, B. Bhaduri, H. E. Kondakci and A. F. Abouraddy, Classification of propagation-invariant space-time wavepackets in free spac: Theory and experiments, *Phys. Rev. A* **99**, 023856 (2019).
- [32] K. Reivelt and P. Saari, Experimental demonstration of realizability of optical focus wave modes, *Phys. Rev. E* **66**, 056611-1-9 (2002).
- [33] P. Bownan, H. Valtna-Lukner, M. Löhmus, P. Piskarv, P. Saari, and R. Trebino, Measurement of the spatio-temporal field of ultrashort Bessel-X pulses, *Opt. Lett.* **34**, 2276 (2009).
- [34] P. Saari, X-Type Waves in Ultrafast Optics, in [37] pp. 109-134.
- [35] H. F. Kondakci and A. F. Abouraddy, Diffraction-free space-time light sheets, *Nat. Photon.* **11**, 733-740 (2017).electromagnetic localized waves with complex spectra, *Phys. Rev. Appl.* **9**, 054005-1-15 (2018).
- [36] *Localized Waves*, edited by H. E. Hernandez-Figueroa, M. Zamboni-Rached, and E. Recami (J. Wiley, New York, 2007).
- [37] *Non-Diffracting Waves*, edited by H. E. Hernandez-Figueroa, E. Recami, and M. Zamboni-Rached (J. Wiley, New York, 2013).
- [38] M. Yessemov, L. A. Hall, K. L. Schepler and A. F. Abouraddy, Space-time wavepackets, *Advances in Optics and Photonics* **14**, 455-570 (2022).
- [39] P. Saari, Reexamination of group velocities of structured light pulses, *Phys. Rev. A* **97**, 063824 (2018).
- [40] P. Saari, O. Rebane, and I. Besieris, Energy-flow velocities of nondiffracting localized waves, *Phys. Rev. A* **100**, 013849 (2019).
- [41] M. Zamboni-Rached, Unidirectional decomposition method for obtaining exact localized solutions totally free of backward components, *Phys. Rev. A* **79**, 013816 (2009).
- [42] I. A. So, A. B. Plachenov and A. P. Kiselev, Simple unidirectional finite-energy pulses, *Phys. Rev. A* **102**, 063529 (2020).
- [43] I. Besieris and P. Saari, Energy backflow in unidirectional spatiotemporally localized wave packets, *Phys. Rev. A* **107**, 033502 (2023).
- [44] J. Lekner, Family of oscillatory electromagnetic pulses, *Phys. Rev. A* **108**, 063502 (2023). See also: J. Lekner, Erratum: Family of oscillatory electromagnetic pulses, *Phys. Rev. A* (to be published).
- [45] L. Mackinnon, Particle rest mass and the de Broglie wave packet, *Lettere al Nuovo Cimento* **31**, 37-38 (1981).
- [46] L.A. Hall, A.F. Abouraddy, Observation of optical de Broglie-Mackinnon wave packets. *Nat. Phys.* **19**, 435-444 (2023).
- [47] P. Saari and I. M. Besieris, Matters Arising: On physical

- nature of the optical deDroglie-Mackinnon wave packets, <https://arxiv.org/abs/2403.02343>, Febr. 2024.
- [48] M. Yessenov, M. Romer, N. Ichiji, and A. F. Abouraddy, Experimental realization of Lorentz boosts of space-time wave packets, *Phys. Rev. A* **109**, 013509 (2024).
- [49] C. J. R. Sheppard and P. Saari, Lommel pulses: An analytic form for localized waves of the focus wave mode type with bandlimited spectrum, *Opt. Express* **16**, 150-160 (2008).
- [50] *Tables of integral transforms*, edited by A. Erdelyi (McGraw-Hill, New York, 1954), Vol. I.
- [51] J. Lekner, Tight focusing of light beams: a set of exact solutions, *Proc. R. Soc. A* **472**, 20160538 (2016).
- [52] I. S. Gradshteyn and I.M.Ryzhik, *Integrals, Series and Products*, 6th ed. (Academic, New York, 2000). We established that in order to get the right results by the table expression with the Legendre function, the branch cut line for the latter must not be placed outside the segment $(-1, 1)$ of the real axis, which is, however, the common placing, e.g., in WolframAlpha on-line calculator and the default one in the Mathematica package